SDU
University of Southern Denmark

Mapping Charge Carrier Density in Organic Thin-Film Transistors by Time-Resolved Photoluminescence Lifetime Studies

Leißner, Till; Jensen, Per Baunegaard With; Liu, Yiming; Brewer, Jonathan R.; Fiutowski, Jacek; Rubahn, Horst-Günter; Kjelstrup-Hansen, Jakob

Published in:
Organic Electronics

DOI:
10.1016/j.orgel.2017.06.043

Publication date:
2017

Document version
Accepted manuscript

Citation for pulished version (APA):
Leißner, T., Jensen, P. B. W., Liu, Y., Brewer, J. R., Fiutowski, J., Rubahn, H-G., & Kjelstrup-Hansen, J. (2017). Mapping Charge Carrier Density in Organic Thin-Film Transistors by Time-Resolved Photoluminescence Lifetime Studies. *Organic Electronics*, *49*, 69-75. https://doi.org/10.1016/j.orgel.2017.06.043

Terms of use
This work is brought to you by the University of Southern Denmark through the SDU Research Portal.
Unless otherwise specified it has been shared according to the terms for self-archiving.
If no other license is stated, these terms apply:

- You may download this work for personal use only.
- You may not further distribute the material or use it for any profit-making activity or commercial gain
- You may freely distribute the URL identifying this open access version

If you believe that this document breaches copyright please contact us providing details and we will investigate your claim.
Please direct all enquiries to puresupport@bib.sdu.dk

Download date: 29. Nov. 2020

Mapping Charge Carrier Density in Organic Thin-Film Transistors by Time-Resolved Photoluminescence Lifetime Studies

Till Leißner[a,1,*], Per B. W. Jensen[a,1], Yiming Liu[a,1], Jonathan R. Brewer[b], Jacek Fiutowski[a], Horst-Günter Rubahn[a], Jakob Kjelstrup-Hansen[a]

[a]*SDU Nanosyd, Mads Clausen Institute, University of Southern Denmark, Alsion 2, 6400 Sønderborg, Denmark*
[b]*Department of Biochemistry and Molecular Biology, University of Southern Denmark, Campusvej 55, 5230 Odense, Denmark*

Abstract

The device performance of organic transistors is strongly influenced by the charge carrier distribution. A range of factors effect this distribution, including injection barriers at the metal-semiconductor interface, the morphology of the organic film, and charge traps at the dielectric/organic interface or at grain boundaries. In our comprehensive experimental and analytical work we demonstrate a method to characterize the charge carrier density in organic thin-film transistors using time-resolved photoluminescence spectroscopy. We developed a numerical model that describes the electrical and optical responses consistently. We determined the densities of free and trapped holes at the interface between the organic layer and the SiO_2 gate dielectric by comparison to electrical measurements. Furthermore by applying fluorescence lifetime imaging microscopy we determine the local charge carrier distribution between source and drain electrodes of the transistor for different biasing conditions. We observe the expected hole density gradient from source to drain electrode.

Keywords: Organic thin-film transistors, charge carrier density, time-resolved photoluminescence spectroscopy, fluorescence lifetime imaging microscopy

1. Introduction

Organic Thin-Film Transistors (OTFTs) form the basis for a wide range of applications in both electronics and optoelectronics [1]. These include electrical logic circuits such as ring oscillators and latches [2], active-matrix driver circuits for LED displays [3], light-emitting-transistors (OLET) [4], optical sensors [5] and bio sensors [6]. For all these devices the charge carrier distribution in the organic semiconductor (OSC) layers is crucial to the output from the device, such as output current or emitted light intensity. Using the gradual channel approximation the local charge density in an OTFT can be approximated by fitting to current-voltage (I-V) measurements [7]. However this approach is to some extent inaccurate since it fails to take into account several factors affecting the local charge density such as charge traps in the OSC as well as the OSC/dielectric interface [8, 9], and injections barriers between the OSC and the electrodes of the transistor [10]. Experimentally there are several approaches to determine the local charge density. Bürgi et al. used scanning Kelvin probe microscopy to extract the local charge density in F8T2 transistors [11]. This approach is rather time consuming being a scanning probe technique and requiring vacuum conditions. Koopman et al. recently used a confocal photoluminescence electro-modulation microscopy method to extract the charge density within the channel of a PTCDI-C13-based OTFT [12]. But this method only takes the photoluminescence (PL) intensity into account leaving the precision of the results vulnerable to bleaching of the OSC.

In this work we demonstrate a method that allows the local charge carrier density to be imaged based on its influence on the local PL lifetime. The PL lifetime from an optically stimulated population of excitons is affected by the presence of polarons through exciton-polaron quenching allowing the local polaron density to be determined from optical measurements. We demonstrate the potential of our method through experimental studies of a model transistor device based on an 5,5-bis(naphthyl)-2,2-bithiophene (NaT_2) thin film using electrical and optical characterization methods. First, we present experimental results from time-resolved photoluminescence spectroscopy (TR-PLS). These data indicate clearly that the PL lifetime depends on the bias conditions. In order to quantify the charge carrier density we developed a numerical model that enables us to predict both the PL lifetime and the electrical current-voltage (I-V) characteristics. We used I-V measurements to validate the model. Subsequently, we applied the model to experimental PL results and show that the same numerical model is also capable to model the lifetime response. Finally, we performed fluorescence lifetime imaging microscopy (FLIM), providing lateral resolution, to monitor the local charge carrier density between the source and drain electrodes.

*Corresponding author
Email address: till@mci.sdu.dk (Till Leißner)
[1]These authors contributed equally.

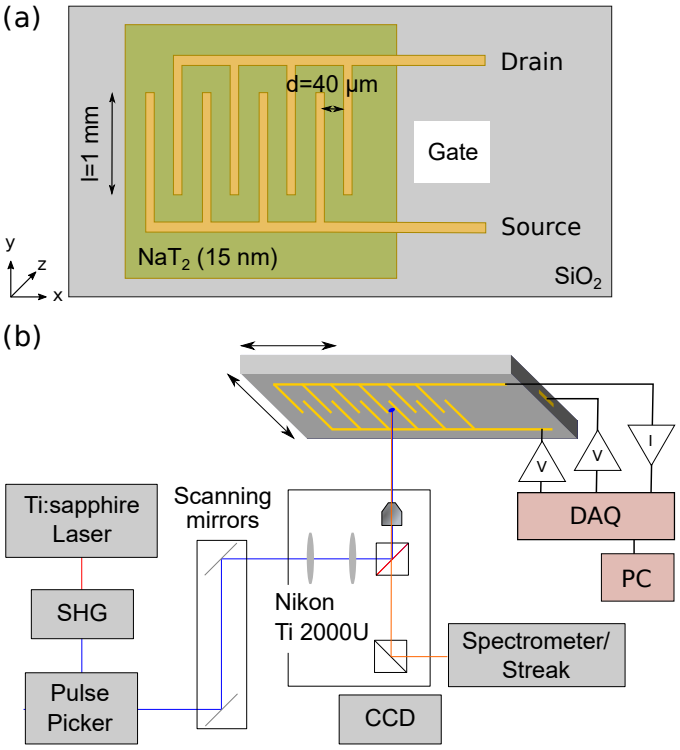

Figure 1: (a) OTFT design; (b) experimental setup for TR-PLS.

2. Methods

2.1. Sample preparation

Fig. 1(a) shows the transistor design based on a doped Si substrate acting as the gate electrode with a 300 nm layer of insulating SiO_2 acting as gate dielectric. An interdigitated array of source and drain electrodes is prepared by UV lithography, titanium/gold deposition, and lift-off. Secondly, the contact to the gate electrode is realized by etching through the SiO_2 layer to the underlying Si substrate. Finally, the substrate is covered with a 15 nm layer of NaT_2 deposited by vacuum sublimation. More details about NaT_2 and sample fabrication are given elsewhere [13]. The distance between source and drain electrodes (channel length) is $d = 40\,\mu m$. The sample is designed to fit a standard Zero Insertion Force (ZIF) socket for easy connection to electrical measurement equipment.

2.2. Time-resolved photoluminescence spectroscopy

TR-PLS was conducted with a home-built laser scanning microscope combined with a streak camera system for temporal and spectral resolution as illustrated in Fig. 1(b). The TR-PLS setup utilizes the frequency-doubled output using a commercial second harmonic generator (HarmoniXX, APE) of a Ti:Sapphire laser (Tsunami, Spectra-Physics) with a central wave length of $\lambda = 795\,nm$. The initial repetition rate of 75 MHz is reduced by a pulse picker (pulseSelect, APE) to ca. 4 MHz to match the requirements of the streak camera (Streak scope C10627, Hamamatsu). After passing the laser-scanning setup the beam is focused on the sample using a 40× microscope objective (NA= 0.65). The PL signal is collected either by a CCD camera or by the streak camera. Spectral resolution is achieved by having a spectrometer (SpectraPro SP-2300, Princeton Instruments) in front of the streak camera. This setup enables us to perform time-resolved spectroscopy with a temporal resolution of about 25 ps and with diffraction limited lateral resolution. The data was acquired using the HPDTA software by Hamamatsu.

In order to bias the transistor simultaneously with PL lifetime measurements, we designed a special sample holder: We connected the OTFT via a ZIF socket mounted on a printed circuit board (PCB) of the size of a standard microscope glass slide. We recorded the I-V data using a Labview controlled characterization system based on a National Instruments data acquisition card (DAQ) and voltage and current amplifiers.

2.3. Fluorescence lifetime imaging microscopy

For fluorescence lifetime imaging microscopy (FLIM) we used a custom-built two-photon laser scanning setup based on a Nikon Eclipse TI microscope and a Mai Tai DeepSee Ti:Sapphire laser (Spectra Physics). The repetition rate was 80 MHz and the central wavelength was set to $\lambda = 780\,nm$. The laser light was polarized linearly. We acquired PL lifetime images by time-correlated single-photon counting (TCSPC) using high-speed hybrid detectors (HPM-100-40, Becker&Hickl) with a temporal resolution of about 70 ps. The fluorescence signal passed a multiphoton short-pass filter (700 nm) to block any scattered or reflected laser light. Then the signal was split by a dichroic mirror (long-pass 570 nm) in front of the detectors and further filtered by two band pass filters in front of the detectors (detector 1: $(607 \pm 40)\,nm$, detector 2: $(542 \pm 10)\,nm$) to measure the distinct lifetimes for the two pronounced peaks in the NaT_2 spectrum. The setup is described in detail elsewhere [14, 15]. We used an acousto-optical modulator triggered by the laser-scanning electronics to adjust the laser power and to ensure that the sample is illuminated only during data acquisition. The biasing of the sample is fully software controlled and synchronized with the FLIM acquisition software.

2.4. Numerical model

The PL lifetime is directly related to the exciton lifetime [16]. The exciton lifetime is assumed to be influenced by local charge carriers, which act as quenching centers, and is described through the Stern-Volmer formula [17, 12]:

$$\frac{1}{\tau} = \frac{1}{\tau_0} + 4\pi r D \rho \qquad (1)$$

where τ is the exciton lifetime extracted from measurements, τ_0 is the exciton lifetime of pristine material, r is the sum of the exciton and hole radii, D is the exciton diffusion coefficient, and ρ is the local charge density that varies at different bias voltages. In order to reveal the values of ρ and thus interpret the exciton lifetime measurement data, we employed a two-dimensional time-dependent drift-diffusion model to simulate the OTFT device behavior [18]. It was found that a hole-trapping defect can explain the threshold voltage shift and the hysteresis observed in experimental transfer characteristics [19]. In our model, we

assume the hole-trapping defect is located at the interface between NaT_2 and SiO_2 [9], and the surface-density σ of the interface defect can be extracted from the threshold voltage shift ΔV_t by [20]:

$$\sigma_{if} = \epsilon \frac{\Delta V_t}{d} \tag{2}$$

where ϵ and d are the permittivity and thickness of SiO_2, respectively. The holes trapped by the interface defect are not fixed, but follow the Shockley-Read-Hall statistics [20, 21]:

$$\begin{aligned} \frac{df_t}{dt} &= (\sigma_p V_{th} p + \sigma_n V_t n_t) \\ &\quad - f_t(\sigma_p V_{th}(p + p_t) + \sigma_n V_{th}(n + n_t)) \end{aligned} \tag{3}$$

where f_t is occupation probability of holes trapped by the defect, V_{th} is the carrier thermal velocities, n and p are carrier densities, σ_n and σ_p are capture cross-section areas, and n_t, p_t are defect characteristic density for electrons and holes, respectively. In our analysis, the parameters σ_n and σ_p are adjusted for fitting the hysteresis amplitudes. The hole mobility can be extracted from the experimental transfer characteristics using the gradual channel approximation [7]. Though, the hole mobility was used as a fitting parameter for matching the transfer characteristics, because in NaT_2, the local charge density ρ consists of the free and trapped hole densities. Trapping and de-trapping processes are not taken into account in the gradual channel approximation, but will be quantitatively revealed by the simulation.

3. Results and discussion

Fig. 2 shows experimental TR-PLS results. A streak trace from a pristine NaT_2 OTFT is shown in Fig. 2(a). The gate electrode is unbiased (V_g = 0 V), while a source-drain voltage of V_{ds} = −30 V is applied. The horizontal axis shows the wavelength of the PL photons and the vertical axis shows the arrival time of the photons. The PL decay time of the transistor is very short and most photons arrive within the first nanosecond after laser excitation. However, a time range of 5 ns was chosen for the experiments in order to ensure a proper fitting of the lifetime data. The monitored spectral range is in total from 485 to 575 nm. A temporal integration of the data yields the spectrum of the device as shown in Fig. 2(b). To prevent bleaching effects long exposure times were avoided. Thus the peaks observed earlier from NaT_2 thin films [13] are not pronounced. For lifetime analysis we consider one of the main peaks in the NaT_2 spectrum from ca. 525 to 545 nm as illustrated by the white lines in Figure 2(a). This region of interest is shown in Figure 2(c). In order to analyse the lifetime we spectrally integrate this data. The resulting decay curve is shown in black. To determine the PL lifetime we performed a two-exponential fit of the intensity decay data $I(t)$ using a Python fitting routine using following model:

$$I(t) = A\left[a_1 \exp\left(\frac{-t}{\tau_1}\right) + a_2 \exp\left(\frac{-t}{\tau_2}\right)\right] \tag{4}$$

where τ_1 and τ_2 are the time constants and a_1 and a_2 are the corresponding relative amplitudes and A is the total amplitude. The instrument response function (IRF) was measured separately and considered within the fitting procedure. From the fit we get τ_1 = 0.27 ns and τ_2 = 1.26 ns with a relative amplitude of a_1 = 68 % of the total amplitude A. The error of the fit of the decay times is smaller than 0.02 ns. The fit is shown as red curve in Fig. 2(c). The absolute PL lifetime values are similar to lifetimes reported for other thiophene-based molecules [22].

After we determined the PL lifetime for V_g = 0 V, where we expect no additional charge carriers to be present between the source and the drain electrode, we subsequently applied different gate voltages (V_g = 0, −30, −40 and −50 V) at a constant drain-source bias of V_{ds} = −30 V. Fig. 2(d) shows the region of interest of the streak trace for V_g = −50 V. It is clearly visible that the decay is shorter than for the unbiased sample. This can be explained by the increased presence of charge carriers in the transistor channel. The quantitative analysis of the decay curve yields τ_1 =0.27 ns and τ_2 =1.08 ns with a relative amplitude of a_1 = 72 %. Before describing the results further, we want to note, that it turns out by analyzing the data for various bias settings, that a_1 = (70 ± 2) % and τ_1 = (0.27 ± 0.01) ns. Thus, for the following analysis τ_1 and a_1 were fixed to 0.27 ns and 70 %, respectively. The fact, that we observe a fast decay component, that is independent on the sample bias, can be explained by some experimental artefacts like scattering of stray light into the detector. Furthermore, double exponential decays have been also observed earlier, depending strongly on the exact molecular design and the surrounding [23]. However, in the following only relative changes in the lifetime will be considered since they are, according to the model, related to relative changes in the charge carrier density.

The PL lifetime results of the decay component τ_2 for V_g = 0 V, −30 V, −40 V and −50 V, are summarized in Fig. 3. In panel (a) the PL lifetime as a function of the gate voltage is shown as black symbols. The lifetime decreases with decreasing V_g from initially τ_2 = 1.25 ns at V_g = 0 V to τ_2 = 1.05 ns to 1.20 ns at V_g = −50 V. For each bias condition, the PL decay data was measured four times before the gate electrode was electrically grounded and a reference PL measurement was made to confirm that no sample degradation had occurred. Between each measurement the sample was moved by approx. 30 µm within a single channel of the transistor in order to minimize local photo bleaching effects. Previous experiments showed that the PL lifetime is constant within the fitting error of 0.02 ns for several positions within a channel because of the homogeneity of the NaT_2 thin film. Only for V_g = −50 V a distinct spread of the lifetime is observed, potentially due to local defects in the NaT_2 film. These finding give clear evidence that the applied bias results in an induced carrier density that causes photo-exited excitons to recombine faster.

In order to demonstrate the validity of our numerical model we used it to fit the measured the I-V transfer characteristics of the NaT_2 OTFT. We obtained I-V curves by measuring the drain current I_d while sweeping the gate voltage V_g from 0 V to −50 V and back at a constant drain-source voltage V_{ds} = −30 V. The

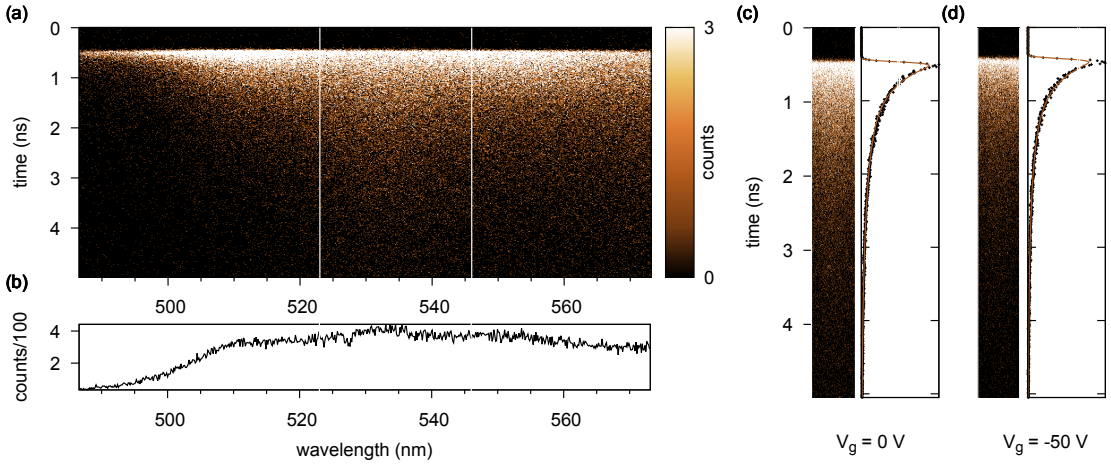

Figure 2: TR-PLS results of a NaT_2 transistor. (a) The streak trace of an OTFT at $V_g = 0$ V. The white lines mark the region of interest (ROI) considered in the data analysis; (b) the spectrum obtained by temporal integration of the streak data; (c) the ROI for a NaT_2 transistor kept at $V_g = 0$ V, the decay curve (black) and the lifetime fit (red); (d) the same NaT_2 transistor biased with $V_g = -50$ V. In all cases $V_{ds} = -30$ V.

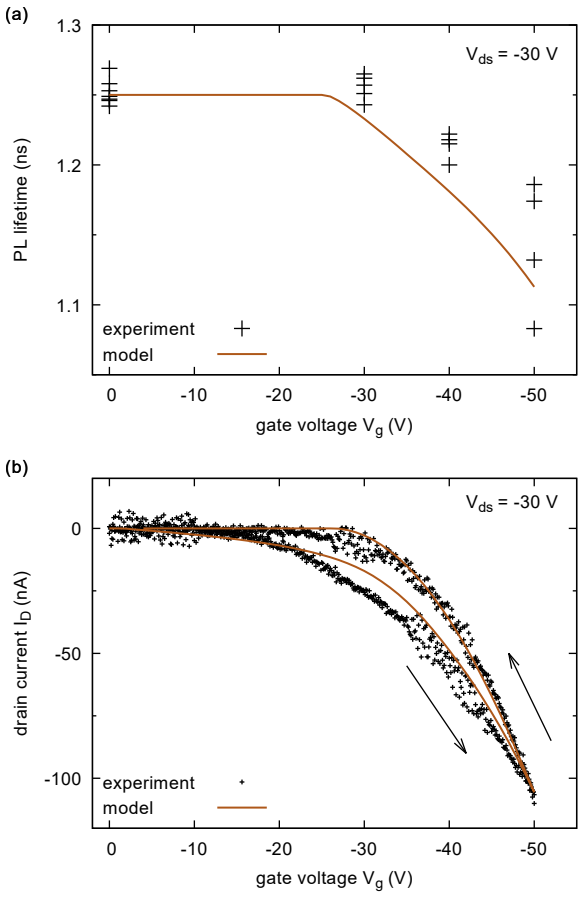

Figure 3: (a) TR-PLS results for various bias conditions. The PL lifetime was determined for gate voltages $V_g = 0$, -30, -40 and -50 V at $V_{ds} = -30$ V. The PL lifetime, shown as black symbols, depends on the gate voltage, i.e. it decreases with decreasing V_g from initially $\tau_2 = 1.25$ ns at $V_g = 0$ V to $\tau_2 = 1.05$ ns to 1.2 ns at $V_g = -50$ V. (b) Experimental and numerical I-V transfer characteristics of the OTFT.

experimental I-V curve is shown in Fig. 3(b) as black symbols. The observed hysteresis is well-known for OTFT [9, 24, 7] and is caused by a shift of the threshold voltage due to trapped charges at the OSC/dielectric interface. This behaviour is in good agreement with OTFT exposed to prolonged bias-stress [25].

According to the gradual channel approximation, we found that the transistor works in the saturated regime and the hole mobilities show only little variation for a gate voltage well above the threshold voltage [26]. In average, the hole mobility is $(1.49 \pm 0.14) \times 10^{-5}$ cm^2/V/s. Because of the small standard deviation, it is justified to consider the hole mobility independent of the gate voltage in the further analysis.

The orange curve in Fig. 3(b) shows the modelled drain current calculated by our numerical model. In our fitting procedure we found a hole mobility of 6×10^{-5} cm^2/V/s, that is around four times higher than the estimate from the gradual channel approximation. We believe that this is due to the fact that during the voltage sweep from the off to the on state of the transistor, the number of trapped holes increase and hence the number of free holes is lower than predicted by the gradual channel approximation. Consequently, a higher mobility is required in the model to fit the measured data. All parameters used in the further analysis are listed in Table 1.

Next to the hole mobility, we found a density of trapped charges of 2×10^{12} cm^{-2}. This value is in good agreement with value reported for similar devices [9, 24]. In summary, the good fit between model and experiment shows the validity of the transient model we have developed in this work.

Afterwards, the PL lifetime trend was fitted by the numerical model described above in order to quantify the charge carrier density. The modelled data is shown as a orange line in Fig. 3(a). It is observed that the experimental PL lifetime data is in good agreement with the model. Both the threshold voltage and the relative change of the lifetime can be reproduced quantitatively. Since the measured exciton lifetime is an effective value arising from the quenching effects at all the depths and all the

Parameters	Drain/Source (Gold)	Gate (n-Si)
Work function (eV)	5.1	4.1
	NaT_2	SiO_2
Relative permittivity	2.56	3.9
Electron affinity (eV)	2.3	0.95
Band gap (eV)	2.2	9
Effective density of states for conduction and valence bands (cm^{-3})	2×10^{21}	10^{22}
Mobility of electrons ($cm^2V^{-1}s^{-1}$)	10×10^{-10}	1
Mobility of holes ($cm^2V^{-1}s^{-1}$)	6×10^{-5}	1
Doping (cm^{-3})	intrinsic	intrinsic
	Interfacial defect between NaT_2/SiO_2	
Defect density (cm^2)	2×10^{12}	
Energy level (eV)	mid-gap	
Capture cross-section (cm^2)	10^{-27} for electrons [27], 10^{-25} for holes	

Table 1: Simulation parameters for OTFT

V_g(V)	p (cm^{-3})	ρ_{eff} (cm^{-3})
0	1.03×10^{-3}	3.38×10^{17}
-10	3.76×10^{-3}	3.38×10^{17}
-20	4.82×10^{-3}	3.38×10^{17}
-30	1.09×10^{17}	4.26×10^{17}
-40	3.95×10^{17}	7.15×10^{17}
-50	6.75×10^{17}	1.66×10^{18}

Table 2: Simulated effective free hole density p_{eff} and local charge densities ρ_{eff}. Other parameters used in Eq. 1 are $r = 1\,\text{nm}$, $D = 1 \times 10^{-4}\,\text{cm}\,\text{s}^{-1}$ [13], and the value of τ_0 is fitted as 1.32 ns.

positions of NaT_2, the local charge density ρ used in Eq. 1 is an effective value that considers the quenching contribution from the overall NaT_2 film thickness, and given by

$$\rho_{\text{eff}} = \frac{\sum_{i,j} \rho_{i,j} \Delta x_i \Delta z_i}{\sum_{i,j} \Delta x_i \Delta z_i} \tag{5}$$

where $\rho_{i,j}$ is the local charge density (including free hole and trapped hole densities) at the node (x_i, z_j), and Δx_i and Δz_i are the grid width and height for the node (x_i, z_j).

From the model we can extract the effective local charge density ρ_{eff} and the effective free hole density p_{eff} for each V_g bias condition when keeping $V_{ds} = -30\,\text{V}$(Table 2) and derive the corresponding exciton lifetime.

In addition to TR-PLS, we used FLIM to study the spatial distribution of the PL lifetime. In the following we used the results of the FLIM detector with the bandpass filter $(542 \pm 10)\,\text{nm}$ in order to be able to compare FLIM and streak results. Fig. 4(a) shows a micrograph of the NaT_2 OTFT. The distance between the two electrodes is again 40 µm, the NaT_2 film thickness is slightly higher than in case of the TR-PLS experiments (21 nm). The image illustrates the homogeneity of the NaT_2 film in-between the source and the drain electrode. A few bright spots are visible, probably caused by some kind of film impurity.

The PL lifetime map for the unbiased device is shown as Fig. 4(b). Here, we are able to use a mono-exponential fit using the same fitting routine as before, taking the instrument response

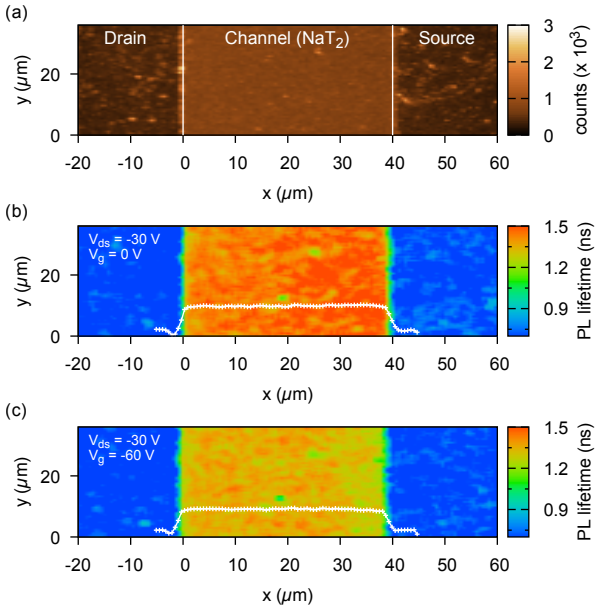

Figure 4: FLIM results: (a) time-integrated signal of the measurement; PL lifetime map of the unbiased transistor at $V_g = 0\,\text{V}$ (b) and at $V_g = -60\,\text{V}$ (c). The white lines illustrate the average PL lifetime between the electrodes found by spatial integrating along the y-axis.

function of the FLIM detection system into account. Before we determined the PL lifetime, we applied a 2-dimensional moving average filter with a filter window of 3x3 px. Due to this, local film impurities, that might act as quenching centres causing a decreased PL lifetime by facilitating radiationless relaxation, appear larger than they are in reality. The spots with short PL lifetimes (shown in green in Fig. 4(b)) seem to correspond to the local defects that are also visible in Fig. 4(a), which are most likely some film impurities.

At the electrodes the PL lifetime is very short (< 500 ns), while in the transistor channel the lifetime is in average τ =1.25 ns, i.e. the quantitative results are in very good agreement with the TR-PLS lifetime results. In Fig. 4(c) the PL lifetime map of the biased device ($V_g = -60\,\text{V}$ at $V_{ds} = -30\,\text{V}$) is shown using the same colour scale as in panel (b). It is clearly visible that the PL lifetime decreased. The insets (white lines) further show the average lifetime along the x-axis, being constant in (b) but showing a gradient in (c). I.e. the local PL lifetime is a function of the distance to the source electrode.

This effect will be analysed quantitatively in the following. Fig. 5(a) shows the experimental results for $V_g = 0\,\text{V}$, $-30\,\text{V}$ and $-60\,\text{V}$ at constant $V_{ds} = -30\,\text{V}$. For $V_g = 0\,\text{V}$ a constant PL lifetime is observed in the transistor channel. As a gate voltage of $V_g = -30\,\text{V}$ is applied, the PL lifetime is shorter and a gradient of the PL lifetime between drain and source electrode is observed. The shorter PL lifetime is found at the source electrode where the holes are injected into the transistor channel and is related to the local charge carrier density. The PL lifetime gradient becomes more obvious when a gate voltage of $V_g = -60\,\text{V}$ is applied. The modelled results for τ are shown in Fig. 5(b), and are qualitatively in good agreement with the experimental data. For $V_g = -30\,\text{V}$, a weak increase of the PL lifetime is

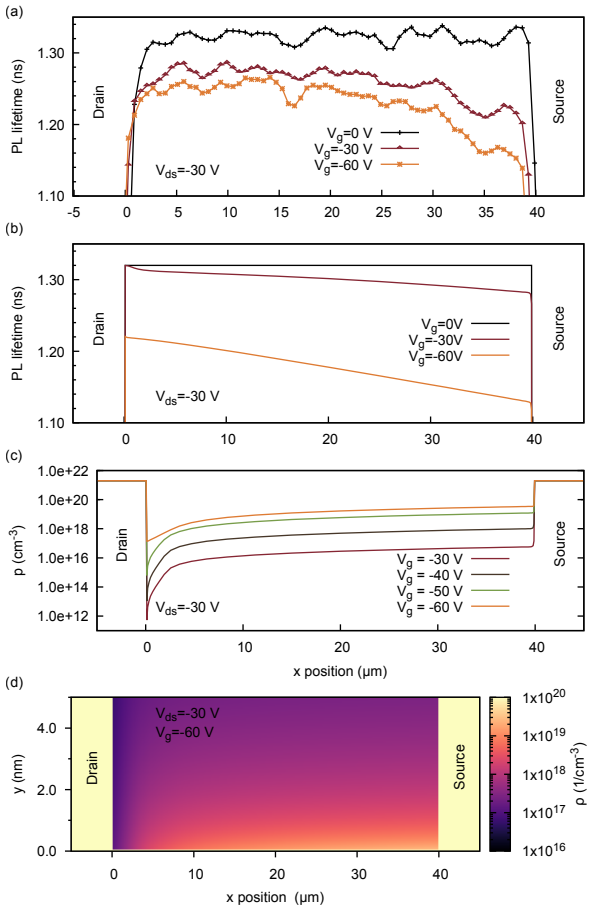

Figure 5: (a) Experimental PL lifetime. The FLIM data was integrated in y-direction before fitting. (b) Modelled lifetime. (c) Free hole density p. (d) 2-d map of the effective charge carrier density ρ.

visible close to the drain electrode, where it coincidence with the value observed for the unbiased transistor. For $V_g = -60\,\mathrm{V}$ data the increase is smaller, but still discernible. This effect can be explained by the existence of a depletion zone close to the drain electrode. To illustrate this, Fig. 5(c) shows the free hole density p. The pinch-off is visible close to of the drain electrode, most pronounced for $V_g = -30\,\mathrm{V}$, where the hole density drops to approx. $10 \times 10^{12}\,\mathrm{cm}^{-3}$. Similar behaviour is seen also for the other gate voltages, but less pronounced. This trend is in good agreement with our expectations, because the pinch-off should be visible when $|V_{ds}| \geq |V_g - V_{th}|$. The same feature cannot be observed in the experimental FLIM data in Fig. 5(a). Most likely, this is due to the limited spatial resolution of the optical system: the depletion zone should extend only around half a micrometer into the channel, and our optical system has a resolution of $0.65\,\frac{\mu\mathrm{m}}{\mathrm{px}}$.

Finally, Fig. 5(d) shows a two-dimensional charge carrier density map $\rho(x,z)$ obtained by our model showing the charge distribution in the NaT_2 film within a distance of 5 nm from the substrate/dielectric interface. So far the charge carrier density along the interface normal is not available experimentally and the results can help to optimize the film thickness in stacked organic devices.

4. Summary

In summary, we have shown that optical measurements of the photoluminescence lifetime decay enables us to determine of charge carrier density in organic thin film transistors and other organic electronic devices during operation. We could show that our numerical model describes consistently both the data obtained from electrical device characterization and from optical methods. We confirmed experimentally that the charge carrier density is directly correlated to the PL lifetime change. By applying our numerical model the effective free hole density and the local charge density can be determined from the experimental characterization.

By combining TR-PLS and FLIM it is possible to analyse the charge carrier density with spectral and spatial resolution. The spatial resolution is important because by monitoring the charge carrier density within the device it will be e.g. possible to locate degradation sites of such devices. The spectral resolution will be highly relevant when multilayer or blended organic semiconductor thin films, as used in organic light-emitting devices or organic solar cells, are investigated, where each material has a different spectral response.

Acknowledgements

Financial support from the SDU2020 program of the University of Southern Denmark and the Fabricant Mads Clausens Fond.

References

[1] H. Sirringhaus, 25th Anniversary Article: Organic Field-Effect Transistors: The Path Beyond Amorphous Silicon, Advanced Materials 26 (9) (2014) 1319–1335. doi:10.1002/adma.201304346.
URL http://doi.wiley.com/10.1002/adma.201304346

[2] S. Mandal, G. Dell'Erba, A. Luzio, S. G. Bucella, A. Perinot, A. Calloni, G. Berti, G. Bussetti, L. Duò, A. Facchetti, Y.-Y. Noh, M. Caironi, Fully-printed, all-polymer, bendable and highly transparent complementary logic circuits, Organic Electronics 20 (2015) 132–141. doi:10.1016/j.orgel.2015.02.006.

[3] B. Peng, X. Ren, Z. Wang, X. Wang, R. C. Roberts, P. K. L. Chan, High performance organic transistor active-matrix driver developed on paper substrate, Scientific Reports 4 (2014) 6430–.
URL http://dx.doi.org/10.1038/srep06430

[4] M. Ullah, K. Tandy, S. D. Yambem, M. Aljada, P. L. Burn, P. Meredith, E. B. Namdas, Simultaneous enhancement of brightness, efficiency, and switching in RGB organic light emitting transistors., Advanced materials (Deerfield Beach, Fla.) 25 (43) (2013) 6213–6218. doi:10.1002/adma.201302649.
URL http://www.ncbi.nlm.nih.gov/pubmed/23963863http://doi.wiley.com/10.1002/adma.201302649

[5] X. Liu, L. Tavares, A. Osadnik, J. L. Lausen, J. Kongsted, A. Lützen, H.-G. Rubahn, J. Kjelstrup-Hansen, Low-voltage organic phototransistors based on naphthyl end-capped oligothiophene nanofibers, Organic Electronicsdoi:10.1016/j.orgel.2014.02.023.
URL http://linkinghub.elsevier.com/retrieve/pii/S1566119914000615

[6] L. Torsi, M. Magliulo, K. Manoli, G. Palazzo, Organic field-effect transistor sensors: a tutorial review, Chemical Society Reviews 42 (22) (2013) 8612. doi:10.1039/c3cs60127g.
URL http://xlink.rsc.org/?DOI=c3cs60127g

[7] J. Zaumseil, H. Sirringhaus, Electron and ambipolar transport in organic field-effect transistors., Chemical reviews 107 (4) (2007) 1296–1323. doi:10.1021/cr0501543.
URL http://www.ncbi.nlm.nih.gov/pubmed/17378616

[8] H. Sirringhaus, Reliability of Organic Field-Effect Transistors, Advanced Materials 21 (38{â}39) (2009) 3859–3873. doi:10.1002/adma.200901136.
URL http://doi.wiley.com/10.1002/adma.200901136

[9] C. Goldmann, C. Krellner, K. P. Pernstich, S. Haas, D. J. Gundlach, B. Batlogg, Determination of the interface trap density of rubrene single-crystal field-effect transistors and comparison to the bulk trap density, Journal of Applied Physics 99 (3) (2006) 34507. doi:10.1063/1.2170421.
URL http://scitation.aip.org/content/aip/journal/jap/99/3/10.1063/1.2170421

[10] D. Natali, M. Caironi, Charge Injection in Solution-Processed Organic Field-Effect Transistors: Physics, Models and Characterization Methods, Advanced Materials 24 (11) (2012) 1357–1387. doi:10.1002/adma.201104206.
URL http://doi.wiley.com/10.1002/adma.201104206

[11] L. Bürgi, T. Richards, M. Chiesa, R. H. Friend, H. Sirringhaus, A microscopic view of charge transport in polymer transistors, Synthetic Metals 146 (3) (2004) 297–309. doi:10.1016/j.synthmet.2004.08.009.
URL http://linkinghub.elsevier.com/retrieve/pii/S0379677904003108

[12] W. W. a. Koopman, S. Toffanin, M. Natali, S. Troisi, R. Capelli, V. Biondo, A. Stefani, M. Muccini, Mapping of charge distribution in organic field-effect transistors by confocal photoluminescence electromodulation microscopy., Nano letters 14 (4) (2014) 1695–1700. doi:10.1021/nl402603c.
URL http://www.ncbi.nlm.nih.gov/pubmed/24611682

[13] X. Liu, I. Wallmann, H. Boudinov, J. Kjelstrup-Hansen, M. Schiek, A. Lützen, H.-G. Rubahn, AC-biased organic light-emitting field-effect transistors from naphthyl end-capped oligothiophenes, Organic Electronics 11 (6) (2010) 1096–1102. doi:10.1016/j.orgel.2010.03.015.
URL http://linkinghub.elsevier.com/retrieve/pii/S1566119910000984

[14] E. K. Sobolewska, T. Leißner, L. Jozefowski, J. Brewer, H.-G. Rubahn, J. Adam, J. Fiutowski, Surface plasmons excited by the photoluminescence of organic nanofibers in hybrid plasmonic systems, in: D. L. Andrews, J.-M. Nunzi, A. Ostendorf (Eds.), Proceedings of SPIE - The International Society for Optical Engineering, Vol. 9884, 2016, p. 98843D. doi:10.1117/12.2227813.
URL http://proceedings.spiedigitallibrary.org/proceeding.aspx?doi=10.1117/12.2227813

[15] T. Leißner, O. Kostiučenko, J. R. Brewer, H.-G. Rubahn, J. Fiutowski, Nanostructure induced changes in lifetime and enhanced second-harmonic response of organic-plasmonic hybrids, Applied Physics Letters 107 (25) (2015) 251102. doi:10.1063/1.4938007.
URL http://aip.scitation.org/doi/10.1063/1.4938007

[16] S. Dimitrov, B. Schroeder, C. Nielsen, H. Bronstein, Z. Fei, I. McCulloch, M. Heeney, J. Durrant, Singlet Exciton Lifetimes in Conjugated Polymer Films for Organic Solar Cells, Polymers 8 (1) (2016) 14. doi:10.3390/polym8010014.
URL http://www.mdpi.com/2073-4360/8/1/14

[17] O. V. Mikhnenko, M. Kuik, J. Lin, N. van der Kaap, T.-Q. Nguyen, P. W. M. Blom, Trap-Limited Exciton Diffusion in Organic Semiconductors, Advanced Materials 26 (12) (2014) 1912–1917. doi:10.1002/adma.201304162.
URL http://doi.wiley.com/10.1002/adma.201304162

[18] M. Gruber, E. Zojer, F. Schürrer, K. Zojer, Impact of Materials versus Geometric Parameters on the Contact Resistance in Organic Thin-Film Transistors, Advanced Functional Materials 23 (23) (2013) 2941–2952. doi:10.1002/adfm.201203250.
URL http://doi.wiley.com/10.1002/adfm.201203250

[19] M. Egginger, S. Bauer, R. Schwödiauer, H. Neugebauer, N. S. Sariciftci, Current versus gate voltage hysteresis in organic field effect transistors, Monatshefte für Chemie - Chemical Monthly 140 (7) (2009) 735–750. doi:10.1007/s00706-009-0149-z.
URL http://link.springer.com/10.1007/s00706-009-0149-z

[20] S. K. Possanner, K. Zojer, P. Pacher, E. Zojer, F. Schürrer, Threshold Voltage Shifts in Organic Thin-Film Transistors Due to Self-Assembled Monolayers at the Dielectric Surface, Advanced Functional Materials 19 (6) (2009) 958–967. doi:10.1002/adfm.200801466.
URL http://doi.wiley.com/10.1002/adfm.200801466

[21] W. Shockley, W. T. Read, Statistics of the Recombinations of Holes and Electrons, Physical Review 87 (5) (1952) 835–842. doi:10.1103/PhysRev.87.835.
URL http://link.aps.org/doi/10.1103/PhysRev.87.835

[22] H. Chosrovian, S. Rentsch, D. Grebner, D. U. Dahm, E. Birckner, H. Naarmann, Time-resolved fluorescence studies on thiophene oligomers in solution, Synthetic Metals 60 (1) (1993) 23–26. doi:10.1016/0379-6779(93)91178-5.
URL http://linkinghub.elsevier.com/retrieve/pii/0379677993911785

[23] F. Ito, T. Nagai, Y. Sota, T. Nagamura, Fluorescence properties of ion pair charge transfer complex with bithiophene group, Journal of Photochemistry and Photobiology A: Chemistry 212 (2-3) (2010) 142–146. doi:10.1016/j.jphotochem.2010.04.007.
URL http://linkinghub.elsevier.com/retrieve/pii/S1010603010001231

[24] C. S. S. Sangeeth, P. Stadler, S. Schaur, N. S. Sariciftci, R. Menon, Interfaces and traps in pentacene field-effect transistor, Journal of Applied Physics 108 (11) (2010) 113703. doi:10.1063/1.3517085.
URL http://scitation.aip.org/content/aip/journal/jap/108/11/10.1063/1.3517085

[25] K. K. Ryu, I. Nausieda, D. D. He, A. I. Akinwande, V. Bulovic, C. G. Sodini, Bias-Stress Effect in Pentacene Organic Thin-Film Transistors, IEEE Transactions on Electron Devices 57 (5) (2010) 1003–1008. doi:10.1109/TED.2010.2044282.
URL http://ieeexplore.ieee.org/document/5443757/

[26] See supplementary information for an analysis of the hole mobility.

[27] S. Locci, Modeling of physical and electrical characteristics of organic thin film transistors, Ph.d. thesis, University of Cagliari (2009).